FINAL REPORT: DE-FG07-01ID14107
July 30, 2004
No Distribution Restrictions

Engineering Radioactive Stents for the Prevention of Restenosis

Principal Investigator: Bruce Thomadsen
Investigators: Robert J. Nickles, Larry DeWerd, Douglass Henderson
Research Assistants: Jonathan Nye, Wes Culberson, Stephen Peterson, Michael Meltsner, Liyong Lin
University of Wisconsin – Madison

Executive Summary

Radiation has become an accepted treatment for the prevention of restenosis (re-blockage) of coronary arties following angioplasty. Radioactive stents could be the easiest method of delivery for the radiation, although clinical trials were disappointing. One likely reason was the choice of ^{32}P as the radionuclide, which fails to match the biological needs of the problem. What radionuclide would perform best remains unknown. This project established the physical infrastructure necessary for a rational investigation to determine the optimum radiological characteristics for radioactive stents in the prevention of restenosis following angioplasty. The project investigated methods to activate coronary stents with radionuclides that spanned a range of energies and radiation types that could provide a mapping of the biological response. The project also provided calibration methods to determine the strength of the stents, an a process to calculate the dose distribution actually delivered to the patient's artery — quantities necessary for any future scientific study to improve the effectiveness of radioactive stents. Such studies could benefit the thousands of patients who receive angioplasty each year.

Achievement of Goals

Straight text is the original Goals Statement for the project; Italics indicates the assessment of the fulfillment of the goal.

Overall Project Goal – To develop the physical basis for optimum use of radioactive stents used to inhibit restenosis following angioplasty. The Project has two parts:

Part 1—Part 1 will have a duration of 3 years and will cover the tasks of: a) developing methods for incorporating various radioactive nuclides with differing properties into/onto arterial stents; b) evaluating the permanence of the labeling and leaching into a blood-like environment; c) differentially activating the stents to deliver a dose distribution that adequately covers the ends of the stent.

All Part 1 goals were achieved.

Part 1 Deliverable — Part 1 of the project will produce two deliverables.

The first will be a stream of radioactive stents to Part 2 of the project.

This was done.

The second deliverable will be a topical report evaluating the characteristics of labeling methods for incorporation of radionuclides into the arterial stents, including a) the feasibility for mass production, b) the leaching characteristics, c) uniformity of radionuclide distribution and d) differentially distributing the radionuclide across the stent.

Year 1 deliverable: a progress report on the items a, b and c., and radioactive stents supplied for Part 2.

This was the presentation at the American Nuclear Society.

Year 2 deliverables: The complete topical report on all items, and radioactive stents supplied for Part 2.

This was the Second Year Progress Report.

Year 3 deliverables: A final report and radioactive stents supplied for Part 2.

This is this report.

Part 2 — Part 2 will have a duration of 3 years and will cover the tasks of: a) Development of a method for calibration of radioactive stents in terms of a dosimetrically useful source strength; b) calculation of the dose distribution from a small piece of active stent wire based on Monte Carlo techniques; development of a calculational technique to establish the dose in a tissue-like medium from a deployed stent; Comparison of the analytical calculation process with a Monte Carlo simulation in several sample cases.

Part 2 goals were achieved except as noted below.

Part 2 Deliverable — Part 2 of the project will produce as a deliverable a topical report including: a) calibration techniques for radioactive stents and a set of proposed national standards; b) suggested assay procedure for end users of radioactive stents to check source calibrations; c) calculational techniques for evaluation of the dose from a deployed stent in a patient; and e) validation of the calculation technique through comparison with Monte Carlo simulations.

Year 1 deliverables: A progress report on the calibration and dosimetry of radioactive stents.

This was the presentation at the American Nuclear Society.

Year 2 deliverables: A final topical report on the calculation of radioactive stents using an air-based extrapolation chamber, and a progress report on the dose distribution from radioactive stents.

This was the Second Year Progress Report.

Year 3 deliverables: The final topical report on calibration of radioactive stents using a liquid-filled extrapolation chamber, and the final topical report on three-dimensional dose-distributions from radioactive stents.

This report presents the final report on the calculational methodology to determine the three-dimensional dose distribution in patients (or experimental animals) in which radioactive stents had been place. The liquid-filled extrapolation chamber was never built, and went through many incarnations over the last year of the project. The necessity for being liquid filled was reconsidered, and the design of an air-filled chamber revised four time. Much has been learned about the chamber design, and a fifth generation chamber is under construction at the time of writing.

Articles and Presentations Related to this Project

Dissertation

S Petersen. Image-based Dosimetry of an Implanted Radioactive Stent using IVUS. July 9, 2004. University of Wisconsin-Madison.

Refereed Publications

SW Peterson, B Thomadsen, Measurements of the dosimetric constants for a new 103Pd brachytherapy source, Brachytherapy 1 (2) 110-119 (2002).

RJ Nickles, TE Barnhart, MA Avila-Rodrigues, AK Converse, R Sundaresan, JA Nye, DW Dick, AD Roberts. Production of 16N2 for Instrument Calibration. Radiochimica Acta (in press)

WS Culberson LA DeWerd, BR Thomadsen, JA Micka, TD Bohm. Calibration of the photon component of 198Au Stents (Submitted to Applied Radiation and Isotopes).

Published Proceedings

JA Nye, DW Dick, MJ Schueller, M Jensen, RJ Nickles. A Cryobuncher Based on a 10-Port Switching Valve. 9th Int'l Workshop on Targetry and Target Chemistry. E10, Turku, Finland, May 23-25, 2002.

JA Nye, DW Dick, RJ Nickles. Pushing the Limits of a 18O Water Target. Application of Accelerator in Research and Industry, 17th Int'l Conf. AIP Preceedings Vol 680, Denton, TX (2002).

AK Converse, JA Nye, TE Barnhart, DW Dick, MA Avila-Rodrigues, R Sundarsan, RJ Nickles, AD Roberts, NH Kalin. MicroPET Performance in the Presence of the Third Gamma. IEEE Nucl Sci Symp (2003) (in press)

Abstracts

S. W. Peterson, B. R. Thomadsen. Concordance Between Disparate Brachytherapy Data Sets. Medical Physics 29:1221 (2002**).**

S Peterson, B Thomadsen. Image-Based Dosimetry for Implanted Radioactive Stents Using IVUS. Med Phys 31: 1891 (2004).

RJ Nickles, AD Roberts, JA Nye, AK Converse, TE Barnhart, MA Avila-Rodrigues, C Dallas, R Sundaresan, DW Dick, RJ Hammes. BR Thomadsen. Assaying and PET Imaging of Yttrium-90 : 1>>34ppm>>0 in IEEE Nuclear Science Symposium and Medical Imaging Conference, October 16 – 22, 2004, Rome, Italy

Presentations

S. W. Peterson, B. R. Thomadsen. Concordance Between Disparate Brachytherapy Data Sets. Annual meeting of the American Association of Physicists in Medicine, Montreal, July 14 – 18, 2002.

WS Culberson, LA DeWerd, BR Thomadsen, JA Nye, JA Micka, KE Stump, SM Beach Calibration of Radioactive Stents. North Central Chapter, American Association of Physicists in Medicine, Minneapolis, November 1, 2002.

WS Culberson, LA DeWerd, BR Thomadsen, JA Nye, JA Micka, KE Stump, SM Beach Calibration of Radioactive Stents. Council of Ionizing Radiation Measurements and Standards. October 21-23, 2002

JA Nye, DW Dick, RJ Nickles. Pushing the Limits of an 18O Water Target. 17th CAARI, Denton, TX (2002)

JA Nye, RJ Nickles. A Visual Study of Beta Ranges. North Central Chapter, American Association of Physicists in Medicine, Madison, WI May 21, 2004.

S Peterson. Image-based Dosimetry for Implanted Radioactive Stents using IVUS. North Central Chapter, American Association of Physicists in Medicine, Madison, WI May 21, 2004.

S Peterson, B Thomadsen. Image-Based Dosimetry for Implanted Radioactive Stents Using IVUS Annual meeting of the American Association of Physicists in Medicine, Pittsburgh, July 25 – 29, 2004.

RJ Nickles, AD Roberts, JA Nye, AK Converse, TE Barnhart, MA Avila-Rodrigues, C Dallas, R Sundaresan, DW Dick, RJ Hammes. BR Thomadsen. Assaying and PET Imaging of Yttrium-90 : 1>>34ppm>>0 Accepted at the 2004 IEEE Nuclear Science Symposium and Medical Imaging Conference, October 16 – 22, 2004, Rome, Italy

Patent Disclosures

#1953 - "A Device to Assist in Implantation of Radioactive Sources Used in Radiotherapy (Brachytherapy) to Treat Disease" – Bruce Thomadsen, Warren D'Souza, Michael Meltsner. 11/15/2002

#2465 - "An Improved System for the Cyclotron Production of I-124" – Jonathan Nye, Robert J. Nickles. 5/21/2004

Background of the Project

Overall Project Goal – To develop the tools to establish the physical basis for optimum use of radioactive stents used to inhibit restenosis following angioplasty.

The Problem Addressed — Following angioplasty (see Figure 1) for coronary stenosis, 60% of patients suffer from a re-blockage of the artery (restenosis). Coronary stents reduce this number to about 40%, but that is still an unacceptably high incidence. Radiation delivered at the time of angioplasty, combined with a stent brings the incidence to about 4%. The most convenient method for delivery of the radiation would be making the stents radioactive. This approach was tried, using ^{32}P as the source material, and while it worked in experimental animals, the results in patients were not nearly as good was with temporarily placing sources in a catheter in the artery (Transcatheter approach). The reason for the failure likely fell with the selection of the radionuclide. While the choice seemed good at the time for several reasons: it was a pure beta emitter, reducing shielding problems; the half-life seemed to match the time course for restenosis; and the manufacture found it relatively easy to manufacture. With the current understanding, the half-life was too long for stopping the restenosis process (the biology leading to restenosis is over in about 4 days) and too short to provide long-time protection. The range may also have been too short to deliver high enough doses to the ends of the injured region.

Project—In order to perform animal experiments to determine the effects of stents labeled with radionuclides of various characteristics, three sets of tools will be required:

1. Manufacture of radioactive stents. To use radionuclides with various characteristics requires labeling the stents with a wide range of elements with vary different chemical properties. This project investigates methods of doing so.
2. Calibration of sources. Once produced, the strength of the sources must be determined. This is not simply the activity contained on the source (the

determination of which is part of the manufacture), but rather a measure of output of radiation related directly to dose delivered to tissue.

3. Calculation of dose. The final step is to determine the dose distribution delivered to the artery wall in an experimental animal. The dose distribution depends not only on the source strength but also the final geometry of the source in situ. This step requires algorithms to link the stent strength and the geometry as defined by imaging.

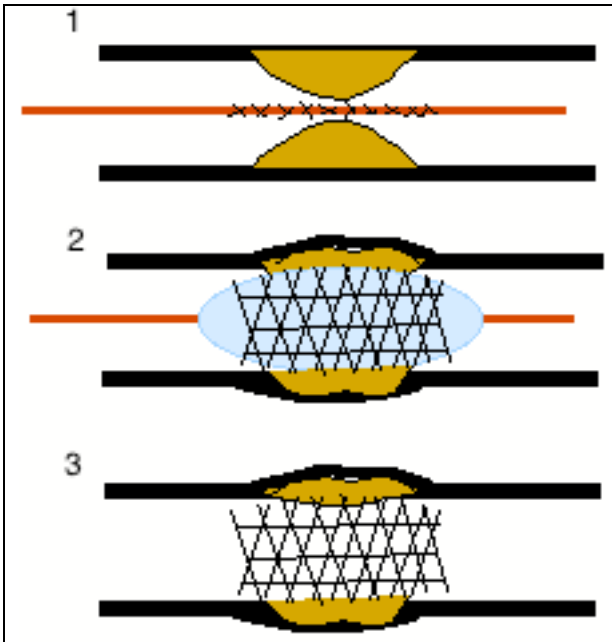

Figure 1. Illustration of angioplasty. 1. The catheter (red) moves into the occluded section of the artery (artery in black; plaque in brown). 2. The balloon (blue) expands, pushing the plaque into the artery wall and opening a channel. 3. After deflating the balloon and removing the catheter, the stent remains in place, expanded to the diameter of the inflated balloon, to hold the artery open.

Results

The project has three sections, each of which runs concurrently, and report below. The sections are those activities necessary to use radioactive stents, manufacture, calibration and dosimetry. The first year was mostly spent establishing the infrastructure required to perform the listed activities. In year two, the team addressed one of the most likely radionuclides for these treatments, ^{198}Au. Year three saw the generalization of the methodologies for applications to stents activated with any of a wide range of radionuclides, and the completion of the model for calculation of the dose distribution resulting for such stents.

Manufacture of radioactive stents

1. Introduction

The goal of the project was to develop radioactive stents using a wide variety of radionuclide engines. It is likely that the radioactive stents used in clinical trials, ^{32}P (which did not work very well), had a half life too long to deliver an adequate dose in the time during which the tissue would be sensitive to radiological intervention (probably 1 to 2 days) and with an energy too low to cover all the injured tissue. However, these assertions remain conjecture until animal experiments can provide data. Such experiments would have to cover radionuclide engines considered likely to provide good therapeutic effects as well as those unlikely to delimit the parameters of the disease.

Activating the stents forms the most challenging part of the manufacturing process, followed by assessing the activity of the radionuclide attached.

The task sequence leading to fabricating of a radioactive stent generally follows the pathway:

- Radioisotope production
- Radiochemical separation of the product from the target material, and
- Plating or implantation of the radioactive material onto the stent substrate.

An example of this sequence is the production of the ^{32}P-loaded stents commercially available for clinical trials, where the ^{32}P was produced by the ^{31}P(n,γ)^{32}P reaction in a nuclear reactor, rather than the conventional production route of ^{32}S(n,p)^{32}P, This mode was chosen in order to have no mass=32 carrier for the subsequent implantation step, which made use of an electrostatic mass separator, which selects the ^{32}P beam on the basis of mass (32 daltons). This ^{32}P beam was directed onto stainless steel (SS 304) stents in the focal plane of the mass spectrometer, thereby embedding the radioactive phosphorous several angstroms beneath the surface, making it permanent under the influence of body fluids.

Part of this project was to investigate the incorporation of radionuclides with a wide range of half-lives and emission types and energies into coronary stents, so that future animal experiments would be able to study the biological nature of coronary irradiation. Table 1 reports on radionuclides studied in this project.

Table 1. Radionuclides studies as radiation engines for coronary stents.

Isotope	**$t_{1/2}$**	**Production**	**Chemistry ->Plate on wire -> Stent**
^{198}Au	4 days	^{nat}Au(n,γ) ^{198}Au	pre-plate on Ni strike over wire or stent
^{52}Mn	5 days	^{52}Cr(p,n) ^{52}Mn	direct irradiation of 304 stainless stents
^{56,58}Co	< 1 yr	^{nat}Fe(p,n) ^{56,58}Co	direct irradiation of 304 stainless stents
^{96}Tc	4 days	^{96}Mo(p,n) ^{96}Tc	direct irradiation of 304 stainless stents
^{99m}Tc	6 hrs	^{99}Mo generator	solvent extraction -> MEK, HV plating
^{18}F	2 hr	^{18}O(p,n) ^{18}F	direct electroplating from H_2 ^{18}O target
^{90}Y	64 hr	commercial	strip from unused radiopharmaceuticals
^{11}C	20 min	^{11}B(p,n) ^{11}C	direct irradiation of BN
^{63}Zn	37 min	^{nat}Cu(p,n) ^{63}Zn	direct irradiation of copper
^{66}Ga	9 hr	^{nat}Zn(p,n) ^{66}Ga	direct irradiation of zinc
^{71}Ge	11 days	^{nat}Ga(p,n) ^{71}Ge	unable to plate.

The dominant work involved the use of gold-plated stents, because ^{198}Au seemed the most promising radionuclide, and, being the first not involving shooting a cyclotron beam on the stent directly, served as a model for the labeling processes. The gold-labeled stents pre-plated a thin layer of gold (≈ tens of μgrams/cm^2) over a nickel over-film ("strike") that prepared a Palmaz-Schatz P-104 stent for the plating bath. Careful massing and microscopy determined the Au-film thickness. The plated stents were then irradiated for carefully timed periods (< 1 hr) in the UW Triga reactor at the Nuclear Engineering Department. Activity was assayed by high resolution gamma spectroscopy with a high purity Ge detector of calibrated efficiency, as well as NaI and liquid scintillator detectors as discussed below. Uniformity of the activity was determined by autoradiography, exposing BaFBr (Ce) phosphor plates, as well as exposure in liquid scintillation recorded by time-lapse microphotography. (See below).

The direct production of radioactive stents with ^{52}Mn, ^{56,58}Co, and ^{96}Tc made use of the proton irradiation of the 304 stainless steel, with Fe, Ni, Cr and Mo constituents. The relative activities of the various radioisotopes can be varied somewhat by the duration of the irradiation and decay periods before use. The irradiation made use of a special stent jig that rotated the cooled stent in the beam of the UW Medical Physics Dept. CTI RDS 112, an 11-MeV proton cyclotron. Again, activity assay employed high-resolution gamma spectroscopy, and uniformity was verified by phosphor plate autoradiography.

Technetium-99m is readily available from commercial generators, retired from a week's service at the UW Nuclear Medicine service. The $^{96}TcO_4^-$ eluate, in 0.9%saline, is made basic with NaOH, and solvent extracted into methyl ethyl ketone. Successful high voltage (400 V DC) electroplating onto stainless steel wires demonstrated the feasibility of stent plating.

In a similar manner, ^{18}F as aqueous fluoride ion is readily made by the proton irradiation of $H_2{}^{18}O$, with a saturation yield of roughly 120 mCi/μA. This aqueous fluoride, with ≈10 nanomole of fluoride carrier, was quantitatively electroplated onto various wires at high voltage (400 V), acting as the anode in a glassy carbon crucible. The distribution of the activity is readily apparent in the time-lapse image of a wire hook immersed in liquid scintillation, shown in the Figure 9c below.

Yttrium-90 could be an attractive candidate for stent plating, and has been studied by the group in Geneva with stents constructed of yttrium wire, then activated in a reactor. Our source of Y-90 comes from unused Y-90 radiopharmaceuticals from our Nuclear Medicine radiopharmacy. The quantitative assay was performed with high purity Ge spectroscopy focusing on the infrequent (34 per million) decays that result in a positron. Similarly, the PET imaging properties of Y-90 were studied in a μ-DeRenzo phantom in our Concorde MicroPET P4 scanner (RJ Nickles, et al, IEEE/MIC Symposium, Rome, 2004), showing that even the infinitesimal positron decay of Y-90 lends itself to quantitative imaging in some cases.

The next three entries of the above table (carbon, zinc and gallium) are not well suited for stent application due to their short lifetimes, but the imaging of the positron dose distribution with immersion autoradiography and microphotography does lend support to the computational exercise of modern Monte Carlo codes. The final entry of ^{71}Ge quite simply did not lend itself to post-irradiation electrochemistry for plating in our hands. Gas phase separation as GeH_4 or $GeCl_4$, followed by ion implantation with a mass separator onto spinning stents is conceivable, but beyond our resources.

Figure 2 shows the relative doses as a function of distance from point sources of some radionuclides, as calculated by Monte Carlo simulations. All of the curves are normalized 0.5 mm from the sources, a distance suggested by AAPM Task Group 60 in Intravascular Brachytherapy as a possible biological target region of interest.[1] The penetrations vary widely, as do the doses near the surface of the stent.

The labeling process also included:

- Assessment of the uniformity of labeling,
- Assessment of the radiation emitted,
- Assay of activity on the stent, and
- Durability of labeling.

The last quantity should not be confused with the strength of the source. The strength relates to the dose generated by the radioactive stent, which while related to the activity of the stent, is not directly related. Assessing the source strength of the stent is the second part of this project, reported below.

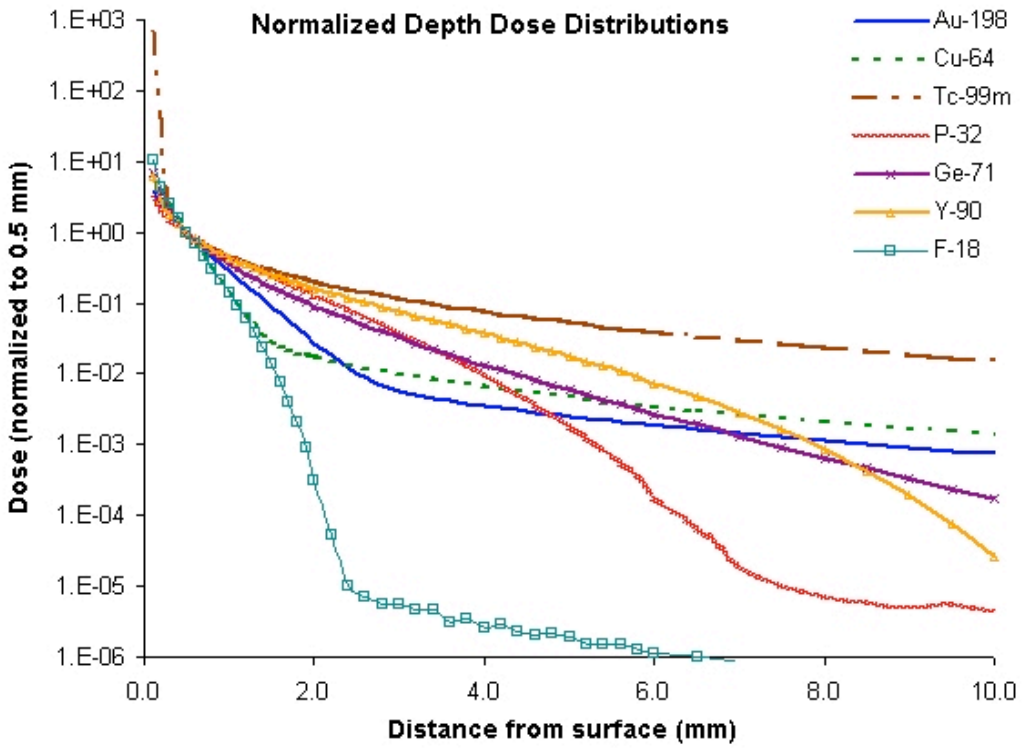

Figure 2. Radial dose distributions from point sources of various radionuclides, normalized at 0.5 mm depth.

The stents used in the project included the Cordis Palmaz-Schatz P-104 Stent, a first generation stent used in most of the labeling experiments and shown in Figures 3 and 4, and the Cordis Palmaz-Schatz Crown stent, a more recent stent shown in Figure 5, used along with the P-104 in some of the imaging and modeling work.

2. Stent Composition

The calibration of the stent depends on the characteristics of the radiation emitted by the stent. The dimensions of the stents are shown in Figure 4. The example shown in Figure 3 is a gold plated stent as described above. This process is cheaper and easier than the production of ^{32}P and there is no real limit imposed on the activity of the ^{198}Au stent.

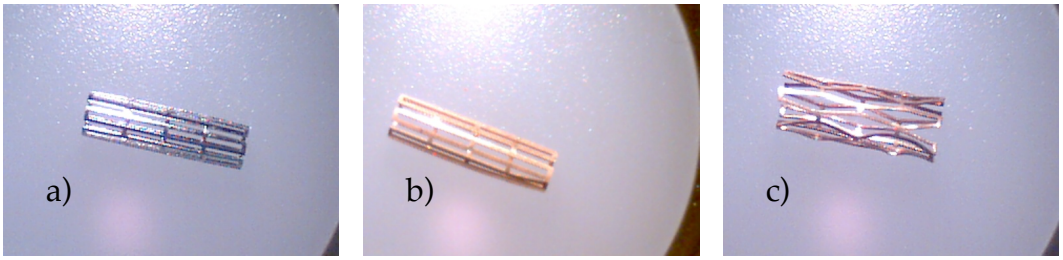

Figure 3. Photos of: a). a bare Palmaz-Schatz P-104stent, b). a gold plated stent, and c). a deployed gold stent.

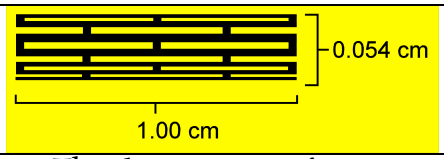

Figure 4. The dimensions of an unexpanded Palmaz-Schatz P-104 stent.

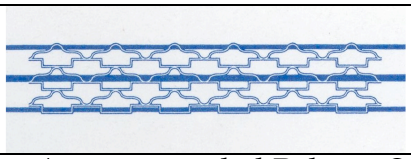

Figure 5. An unexpanded Palmaz-Schatz Crown stent.

3. Isotopic composition.

A stent's spectrum was measured with a high purity germanium (HPGE) detector to determine its isotope composition. The efficiency of the HPGE detector was measured with a standard source traceable to the National Institute of Standards and Technology (NIST) and was applied to find the activity of each isotope present in the stent. Figures 6 and 7 show the spectra of a ^{198}Au stent one day and 50 days after activation. The irradiation produces contaminant radionuclides. It is apparent that the majority of the counts detected one day after activation are from the 412 keV gamma rays emitted by ^{198}Au. It is also apparent that there is ^{51}Cr present in the stent, a result of the stainless steel being activated in the nuclear reactor. One day following activation, the activity of ^{51}Cr is 0.9 % of the activity of ^{198}Au in the stent being measured. The ratio of ^{51}Cr to ^{198}Au present in the stents will vary depending on the amount of electroplated stable gold being activated, the total time in the reactor and the size of the bare stainless steel stent.

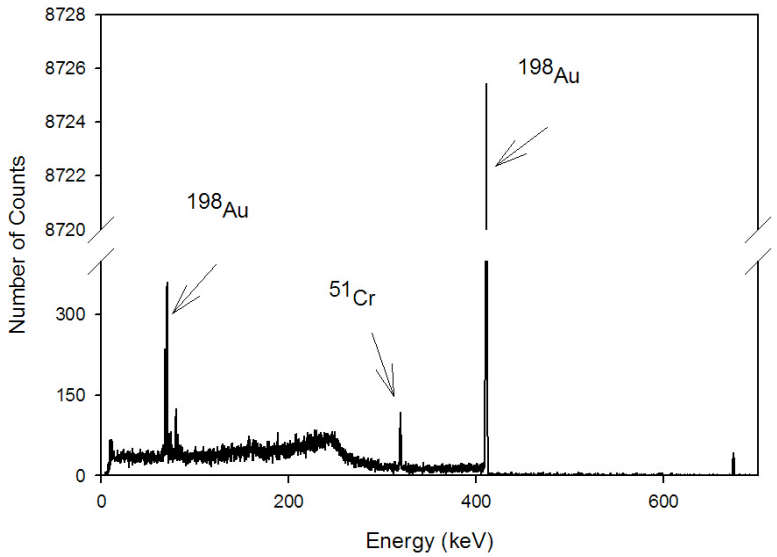

Figure 6. A photon energy spectrum of the stents one day after neutron activation.

Fifty days after neutron activation, the ^{198}Au has decayed more than ten half lives ($t_{1/2}$=2.69 days). The remaining activity in the stent is due to activated stainless steel elements such as ^{51}Cr ($t_{1/2}$=27.7 days), ^{59}Fe ($t_{1/2}$=44.5 days), ^{58}Co ($t_{1/2}$=70.9 days) and ^{60}Co ($t_{1/2}$=5.27years), distinguishable in Figure 7. ^{56}Mn is a product of neutron activated Fe in the stainless steel. With a 2.6-hour half-life, this activity adversely effect the measurements because the technique requires a constant source output during the duration of the measurement. Thus, the stents waited 24 hours after neutron activation before measurements. In clinical applications, the stents would have to be held during this "cooling" time to eliminate the transient activity.

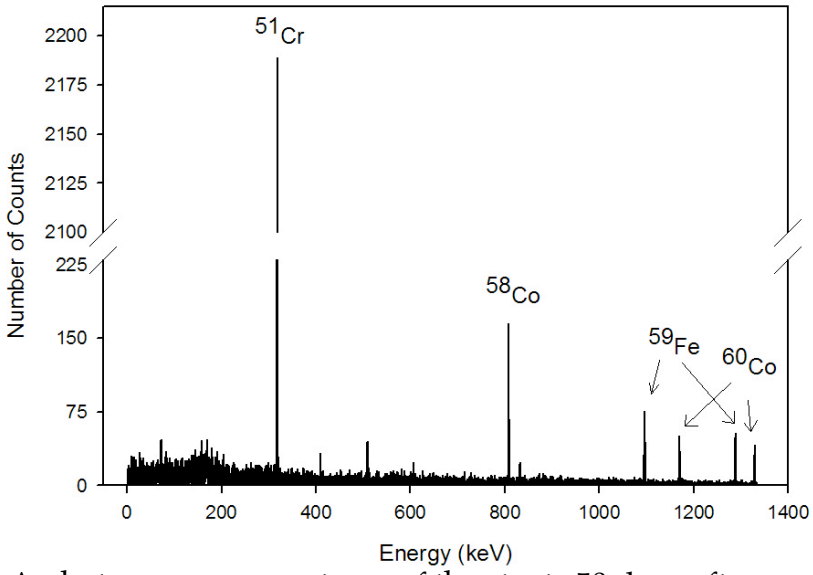

Figure 7. A photon energy spectrum of the stents 50 days after neutron activation.

4. Activity Uniformity

Film Assessment

Contact autoradiography served to assess the electroplating uniformity on the stents. International Specialty Products model HD810 radiochromic film was used with the stent in contact with the film. Following the exposure, the film was placed in an envelope for 24 hours to allow for post-exposure density growth stabilization without the influence of fluorescent lighting. The film was then scanned with a Molecular Dynamics optical scanner (scan resolution of approximately 50 microns) and contour plots were applied. The autoradiographs are normalized to the maximum pixel value for each image and the background of each image was subtracted. Figure 8 shows the result for one of the ^{198}Au stents after exposure for six hours.

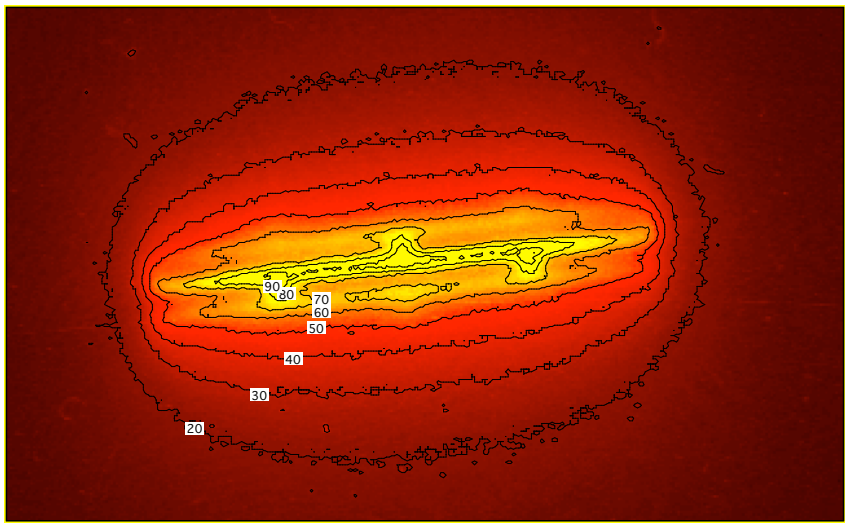

Figure 8. A contact autoradiograph of one of the stents imaged with radiochromic film.

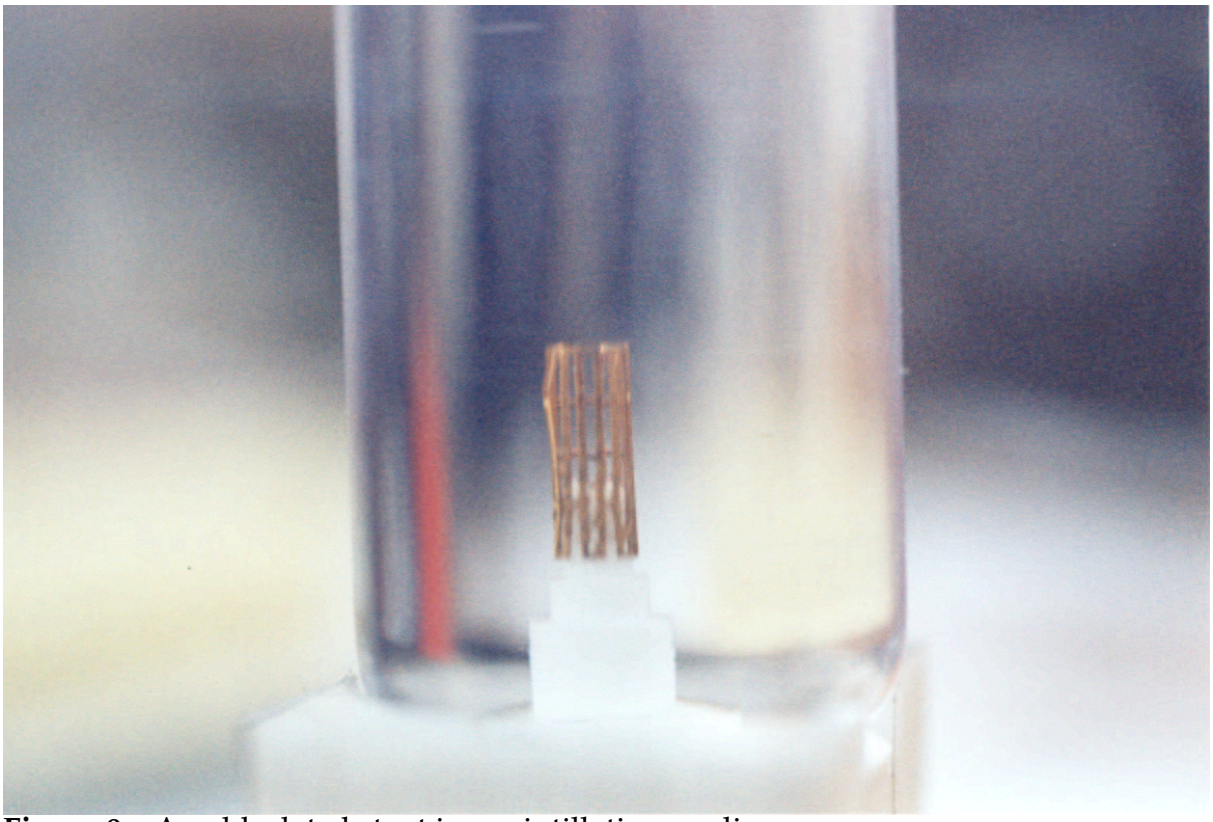

Figure 9a. A gold-plated stent in a scintillation medium.

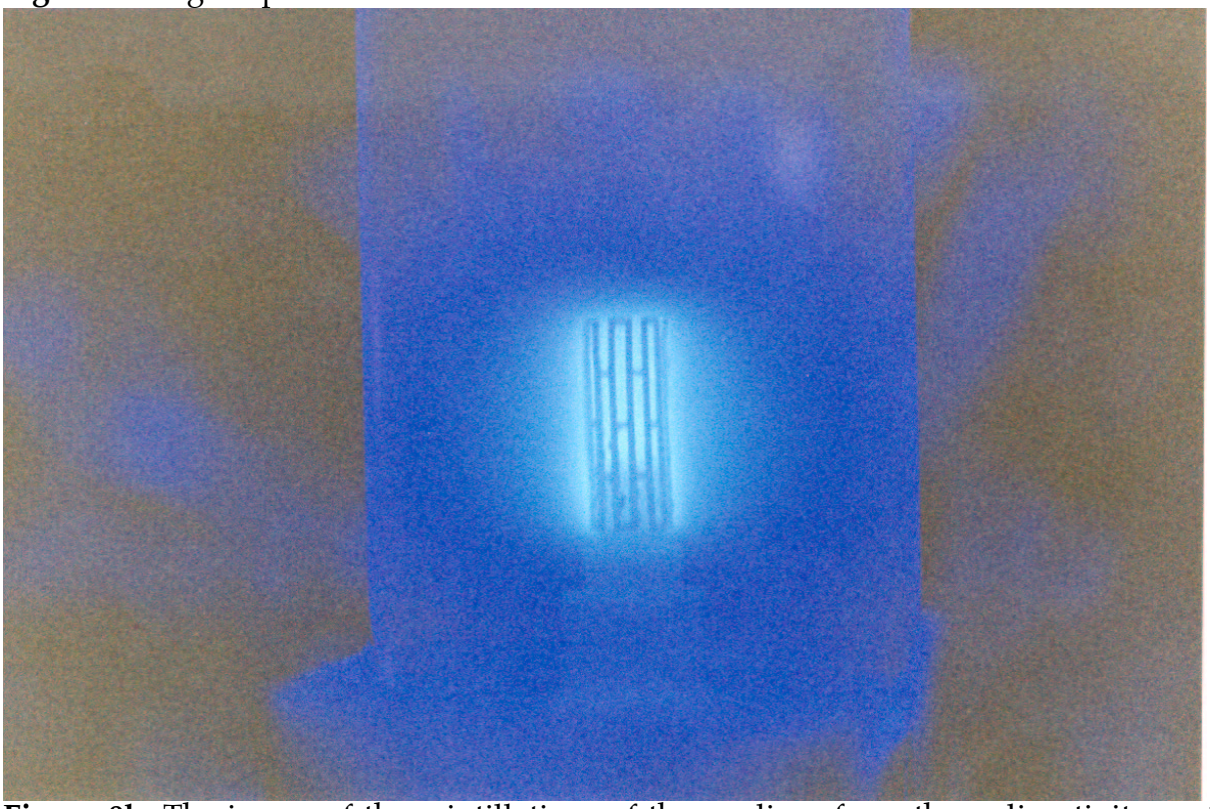

Figure 9b. The image of the scintillations of the medium from the radioactivity on the gold-plated stent shown in Figure 9a.

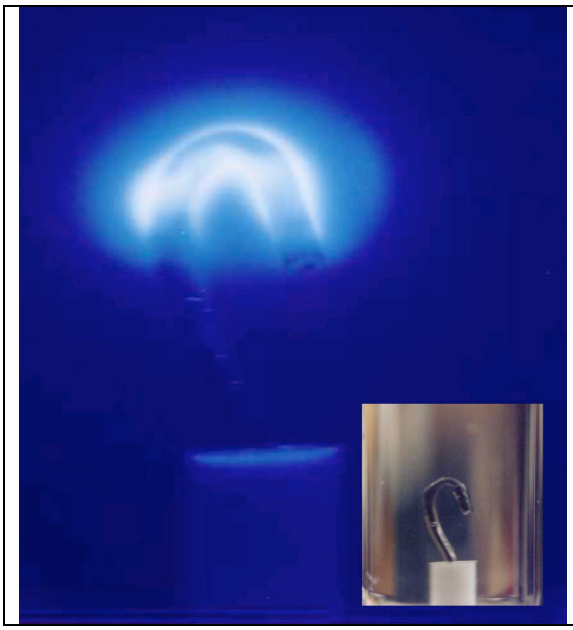

Figure 9c. A photograph of the scintillation around a hooked wire plated with ^{18}F. The insert shows the wire in the scintillation medium in room light.

Liquid scintillation depiction.
A second method to assess the uniformity of the plating of the stent uses liquid scintillation medium. The light output through the medium is proportional to the dose to the medium. The light can be captured by a photographic camera (albeit over a considerable time at the present). Figures 9a shows a normal photograph of a stent in the medium, while Figure 9b shows the image made from the scintillation output. The region of intense dose is apparent.

5. Methods of assessing the activity produced
At the time of manufacture, the activity is determined not for dosimetric standardization, but for manufacture quality control. The standard assay used a well-type ionization chamber (dose calibrator - Capintec CRC-15R), itself calibrated using a set of standards traceable to NIST.

Coincidence counting methods using the b-g coincidence was attempted in the second year of this project. Unfortunately, the geometry of the stent, shielding much of the beta emission in not so straightforward ways, rendered that method infeasible.

Standardization and Calibration of radioactive stents
1. Photon-emitting stent calibration
Calibrating the strength of a photon-emitting stent can follow procedures similar, although not identical, to those used for other photon-emitting brachytherapy sources. These processes could also be applied to mixed beta- and photon-emitting stents by removing the beta component from the radiation observed and then reinserting the electrons during the dose computation. The rationale for taking this approach is that beta particles suffer significant losses in quantity in air, and even greater losses in condensed media, always placing the point of measurement in a large gradient. Photons, on the other hand, undergo relatively slow changes in intensity through attenuation, particularly in air.

The technique used is that developed by Goetsch et al.[2] The method was developed for use with high dose-rate ^{192}Ir brachytherapy units with source strengths three or more orders of magnitude larger than for the stents.
The measurement method involved taking readings at seven distances from the source, and solving the simultaneous equations

$$R_i = \frac{aS_k}{(r_i + r_o)^2} + R_s$$

where R_i is the reading at distance r_i, a is a proportionality constant (calibration factor) between the source strength and the reading on the detector, r_o is an off-set in the distance setup, and R_s is the scatter from the room and the room contents, which should be approximately constant over the range of distances in the experiment. Figure 10 shows the experimental setup.

Readings relatively close to the source suffer from large gradients within the ionization chamber and require correction to give the reading appropriate for the center of the detector.[3,4]

To test the validity of the technique for small-activity sources, the method was first applied to low dose-rate ^{192}Ir sources that had source strengths determined traceably to the NIST and a high dose-rate ^{192}Ir.

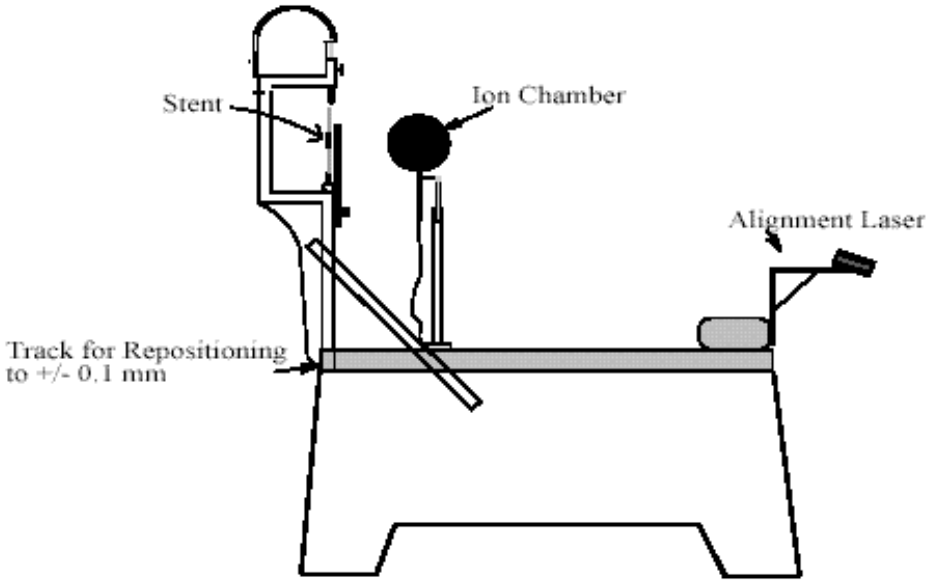

Figure 10. Setup for the in-air determination of the photon source strength.

The measurement used Exradin A3 and A6 spherical ionization chambers. Three measurements were taken with each of the chambers and the results are listed in Table 2. The table shows the average percent difference plus or minus one standard deviation to indicate the distribution of values. The Air Kerma Strength that was determined by the measurement technique is compared the Air Kerma Strength determined by measuring the source with one of the NIST traceable UWADCL standard well chambers. The results agree to the well chamber value within the previously determined overall uncertainty of 2.15%. This shows the reproducibility of these types of measurements as well as the accuracy of making such measurements with the large volume Exradin model A6 ionization chamber.

Table 2. Results from the proof of principle for measuring low activity ^{192}Ir sources with the large volume Exradin A6 chamber.

Source Type	Given Air Kerma Strength	Chamber Used	Chamber Collecting Volume	Number of Trials	Date	Percent Difference from Decayed Well Chamber Value (%)
Varian ^{192}Ir HDR seed	28210 U	A3	3.6cc	2	7/12/2002	-1.50
						-1.56
Varian ^{192}Ir HDR seed	25450 U	A3	3.6cc	1	7/23/2002	-1.42
						-1.49 ± 0.07
Varian ^{192}Ir HDR seed	29270	A6	800cc	3	10/5/2002	0.62
						-0.10
						-0.02
						0.17 ± 0.4
Best ^{192}Ir LDR Seed	13.28 U	A6	800cc	1	7/1/2002	2.13
Best ^{192}Ir LDR Seed	9.795 U	A6	800cc	2	8/5/2002	2.63
						3.23
						2.66 ± 0.6
Best ^{192}Ir LDR Seed	9.172	Inverted A6	800cc	3	8/12/2002	2.31
						2.67
						2.73
						2.57 ± 0.2

The results of this in air measurement technique for ^{198}Au stents are listed in Table 3. Each in-air measured value is listed with its associated uncertainty. The last column shows the measured air kerma strength divided by the activity as measured with a Capintec well chamber. This value is constant over all the measurements to within 3%. Note also that this value closely compares to the value of 2.08 as given in *The Physics of Radiation Therapy*.[5]

Table 3. Results from the measurements of ^{198}Au stents.

Source	Date	Capintec Activity (mCi)	S_k from in-air technique (uGym^2/hr)	St. Dev. / average f-value %	S_k / mCi (U/mCi)
Stent 5	4/23/2003	0.868	1.83 U	5.6%	2.11
	4/24/2003	0.700	1.45 U	1.0%	2.07
	4/25/2003	0.536	1.11 U	1.0%	2.07
Stent 6	4/24/2003	0.613	1.26 U	4.9%	2.05
	4/25/2003	0.479	1.03 U	3.3%	2.16
	4/25/2003	0.444	0.96 U	5.6%	2.16
				Average	2.10 ± .05
				Khan's (uGym^2/mCi-h)	2.08

Table 4. The geometrical dependence on the measured stent strength.

Source Configuration	S_k / mCi (U/mCi)
ST5, normal	2.09
ST5, cut open and flattened	2.16
% difference	3.3%

Since the stent struts are blocking some of the radiation from reaching the detector, it is necessary to investigate the geometrical dependence of this measurement technique. Table 4 shows the result of measuring a closed stent and an open stent. As expected, the measured air kerma strength is slightly higher for the expanded stent. The geometries of each measurement are shown in Figure 11.

The anisotropy dependence of the measurement was also investigated. The charge collected in an Exradin A6 ionization chamber located at 10 cm from the stent was compared for several different angles. The chamber was placed on the perpendicular bisector of the stent and then the stent was rotated 5 times around its longitudinal axis. A drawing of the setup is shown in Figure 12 and Table 5 lists the results. Note that even though there is a 0.5% variation in the angular dependence, there is a 0.6% repositioning uncertainty in the setup. Thus, it is shown that there is no significant anisotropy dependence on the in air measurement technique at a distance of 10 cm.

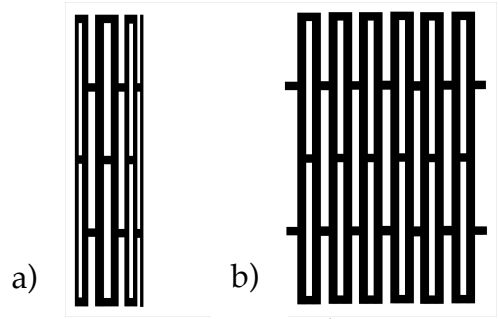

Figure 11. The P-104 stent: a). cylindrical, and b). spread flat.

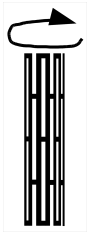

Figure 12. The direction of rotation for the anisotropy measurement.

Table 5. The measured anisotropy dependence of the stent.

Angle (degrees)	Reading (pC)
0°	147.52
90°	147.62
180°	146.63
270°	145.58
360°	146.82
COV (%)	0.5%

2. Beta-emitting stent calibration

In-air becomes less feasible for beta-emitting stents because of the large amount of attenuation and scattering cause by the air. For that reason, measurements close to the stents serve for calibration. While well-type ionization chambers work well for routine

assay, their signal response is too complicated a function to use for a primary calibration tool. For primary calibration, a better device is an extrapolation chamber, an ionization chamber where the electron separation decreases allowing an extrapolation to a zero separation near the stent surface. The National s for Standards and Technology use an extrapolation chamber for the calibration of transcatheter intravascular brachytherapy sources, but that chamber likely would have problems with radioactive stents because the activity falls two orders of magnitude below that normally measured. Additionally, the electron orientation, a flat plate roughly tangential to the surface of the stent, would make extrapolation to the surface difficult. The extrapolation chamber proposed for this project was coaxial to the stent.

Two versions of a cylindrical extrapolation chamber were constructed. The originally constructed model suffered from lack of adequate precision in the construction, which caused variation in results, and shorting (or arcing) problems because of non-rigidity of the central tube. The second design used a conducting plastic for the body of the chamber, but that results in electric field lines that poorly define the collecting region. The third design seems to overcome all the problems encountered and some that were anticipated following the experience with the first two. Figure 13 shows this design.

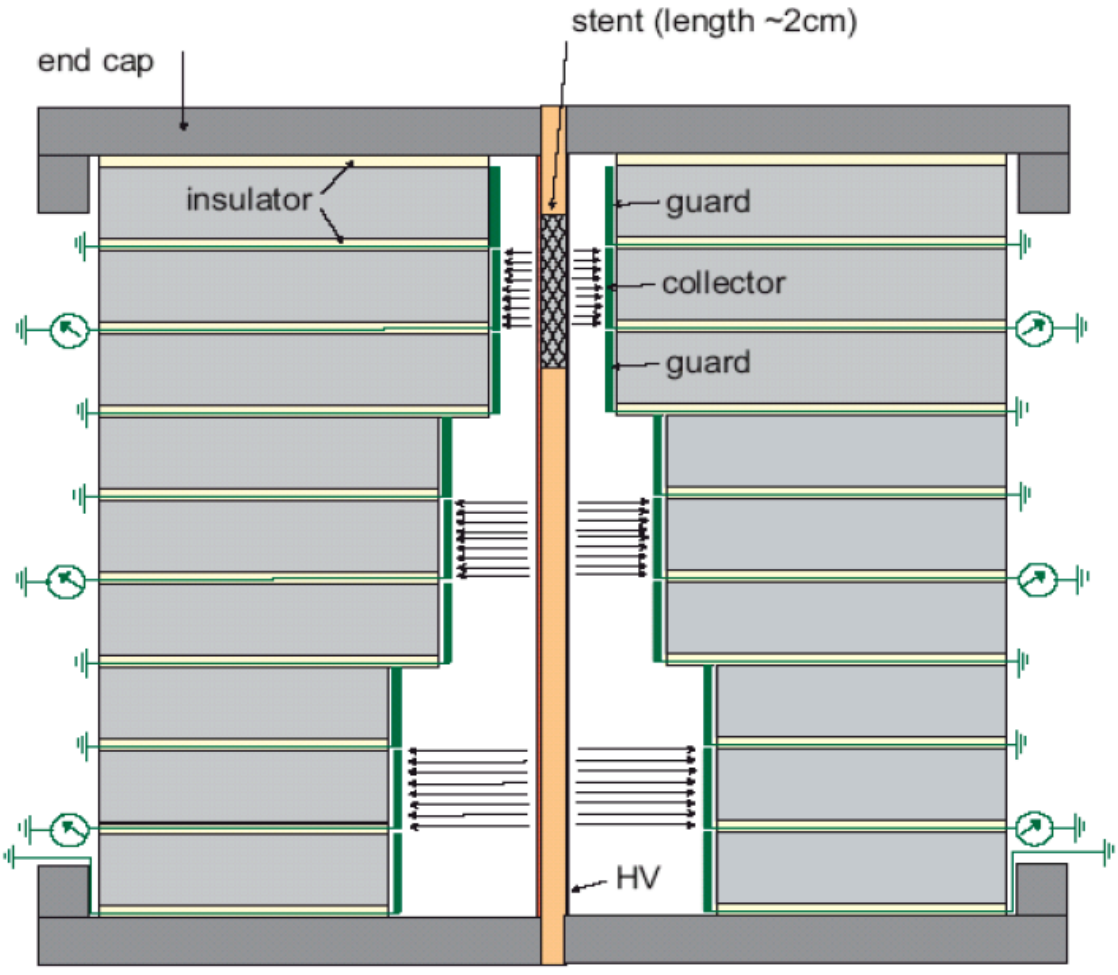

Figure 13: The air-filled extrapolation chamber in a cut-away side view. To better illustrate the concepts, the figure is not to scale.

This design would give a relatively large signal and be less subject to geometric uncertainties. The technique chosen employs an extrapolation chamber with a 4mm diameter hollow center electrode and holder to make current measurements with air gaps ranging from 0.3mm to 2.7mm at 0.4mm intervals. The data should yield a relationship between current and air gap, the slope of which is used to determine the surface absorbed dose rate over the central 60% of the radioactive stent. An ideal center electrode material would be conducting and tissue equivalent, but since we are interested in the absorbed dose rate near the surface of the stent (less than 0.5mm), machining such a material is difficult. Therefore, other materials such as polyimide tubing with conductive coating on its outside surface is more practical. The collector and guard electrodes will be conductive coated, non-conducting tissue-equivalent material.

During the period of the grant, the first three models were built and a fourth proposed, all of which gave raise to the third generation chamber that is now under construction.

Dose distribution calculations

1. Introduction.

The culmination of the project is the calculation of the dose distribution to the artery wall delivered by a radioactive stent. The methodology to be developed was to apply to a stent activated with any radionuclide. Up to now, research and clinical studies published on radioactive stents referred to the source strength in terms of activity in the stent. The levels of radiation outside a stent depend on more than just the activity contains, and the second part of this project addressed the issue of specifying the source strength independently of the contained activity. However, even given a known source strength that relates to the radiation output of the stent, the dose distribution pattern depends on the final geometry of the expanded stent.

Because of the disconnect between the activity of the stent and the resulting dose distribution, any future progress in either animal studies or clinical trials will require careful, detailed dosimetry. The technique developed in this project can serve to provide that information.

2. Calculational Methodology

The approach taken is to begin the dosimetry with an image of the stent in place. The only practical form of imaging at this time is intravascular ultrasound, although in the future improved MR or CT may become feasible for this purpose. The image presents axial section through the artery, showing the struts of the stent in that slice. Due to the complex pattern of the wall of the stent, the parts of the struts may assume unusual shapes. These imaged parts of the struts are called struxels. The general approach to calculating the dose distribution calculates the three-dimensional dose distribution for each struxel and then adds the distributions. While the addition of the distributions follows the normal procedure for a conventional brachytherapy source distribution, the steps leading to that point all require new methodologies. These additional procedures include:

- Characterizing the dose distribution for the struxels, which in turn requires —
    - A Monte Carlo simulation of the dose distribution from struxels of varying sizes and shapes, and
    - Establishing the variables that affect the dose distribution;

- Parameterizing the dose distribution information into a format useful for computerized calculations; and
- A method for describing the spatial distribution of the struxels.

For the development of the calculation procedure, the ^{198}Au stents were used because, and the first labeling radionuclide, we had the most experimental information available. The ^{198}Au also emits both photons and betas, demanding methodologies that address both modalities.

Calculations were performed for both a controlled experimental setup in a phantom for which measurement of dose could be made to compare conformance with the calculations. Calculations were also performed using images from a patient to investigate the feasibility of the methodology in practice.

3. Experiential verification of the model

SOURCES:

The stents used were Johnson and Johnson Palmaz-Schatz P-104 stents made of 316 stainless steel with a length of 1.0 cm and a diameter of 2.6 mm (undeployed). The structure is shown in Figure 1. They were electroplated with ^{197}Au- using a two-step process. The stents were then irradiated in the University of Wisconsin's nuclear reactor, activating the stent by the ^{197}Au(n,γ)^{198}Au reaction. ^{198}Au has a half-life of 2.69 days and decays through beta minus decay to ^{198}Hg, emitting a beta particle with E_{max} of 962 keV and a photon with energy of 412 keV.

VIRTUAL WATER PHANTOM AND RADIOCHROMIC FILM:

Dose measurements from the gold-plated stents were taken using phantoms of Virtual Water™ (MED-CAL Inc., Verona, WI) and GafChromic High Sensitivity (HS) radiochromic film (International Specialty Products, Wayne, NJ). Each phantom was formed from a pair of 12.7 x 14.9 x 5.0 cm Virtual Water blocks. A 10.0 x 10.0 x 0.25 cm hole was machined into each block to hold a 10.0 x 10.0 x 0.5 cm Virtual Water insert. A separate insert was made for each stent size, undeployed (diameter = 2.6 mm) and deployed (diameter = 3.5 to 4.0 mm). The insert held the radioactive stent as well as two pieces of radiochromic film, one in contact and one at either 1 mm or 4 mm away. This structure can be seen in Figure 14. The insert was firmly sandwiched between the two blocks to insure that the positional relationship between the stent and film could be known with little uncertainty, a potential problem due to the difficulty of aligning the stent to the film.

The radiochromic film was calibrated for both beta and gamma radiation. The pixel values were converted into optical density and then the optical density converted into dose. A combination of ^{137}Cs (Energy = 662 keV) and X-ray at 250 kVp was used as the reference for the gamma calibration. To account for the energy dependence of the radiochromic film[6], the response from the ^{137}Cs and X-rays were averaged to get an appropriate energy response for the 412 keV photons of ^{198}Au. Due to the fact that there are no calibrated beta sources that correspond to the beta energy of ^{198}Au (E_{max} = 0.962 MeV), three different sources were investigated for the beta calibration, ^{90}Sr (E_{max} = 2.28 MeV), ^{60}Co (1.173 and 1.333 MeV photons) and 6 MeV electron beam with 1.5 cm of phantom material (2.9 MeV). The ^{60}Co curve was used to determine the film dose based on the TG-55 recommendation[6].

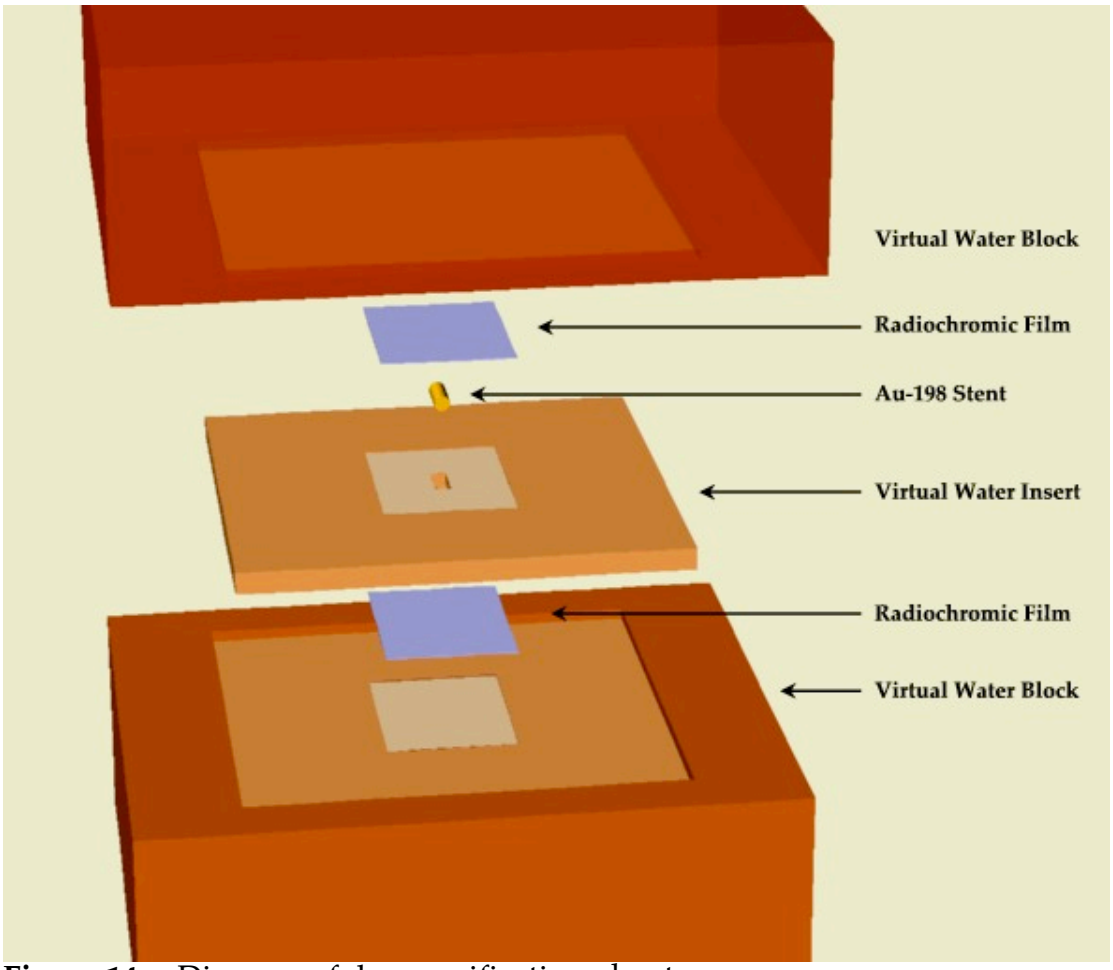

Figure 14. – Diagram of dose-verification phantom

MONTE CARLO SOURCE CALCULATION:

The complete experimental setup was simulated in Monte Carlo, using MCNP4c3. Since ^{198}Au is a dual-particle source, each simulation was run twice, once as a photon source and once as a beta source, with the results from each run being averaged based on the particle emissions. Table 6 gives the frequency of emission per decay. Instead of simulating the entire piece of radiochromic film, slices were calculated along the length of the stent (Z-axis) and across the stent (X-axis). These results are shown in Figure 15 on the next and following pages.

Figure 15 compares the absolute dose results from the radiochromic film measurements and the Monte Carlo calculations. For the data at 1 mm and 4 mm, the correlation is quite good, although the film data at 1 mm in the z direction tapers off due to uneven gold plating on the stent. The data with the film in contact shows a discrepancy between the measured and the calculated. The Monte Carlo calculations show the structure of the stent with peaks at the points of contact, while the radiochromic film has the proper dose values, but without these peaks to show the stent structure. Two possible explanations are that the high dose exposures during measurement compromised the resolution of the film (a known problem) and that there may have been small gaps between the film and the stent, thus blurring the structure. Taken as a whole, the experimental values validate the Monte Carlo methodology.

Table 6. Decay scheme of ^{198}Au

^{198}Au Decay Spectrum							
Betas				Gammas			
source	energy		per 100	source	energy		per 100
	(keV)	(MeV)	particles		(keV)	(MeV)	particles
□- decay	962.000	0.9620	98.990	decay	411.802	0.4118	95.580
□- decay	290.000	0.2900	0.985	decay	675.884	0.6759	0.804
□- decay	1371.000	1.3710	0.025	decay	1087.684	1.0877	0.159
IC	328.700	0.3287	2.882	x-ray	9.989	0.0100	0.457
IC	396.963	0.3970	0.420	x-ray	11.824	0.0118	0.366
IC	397.593	0.3976	0.423	x-ray	11.915	0.0119	0.112
IC	399.518	0.3995	0.188	x-ray	68.894	0.0689	0.801
				x-ray	70.818	0.0708	1.360
				x-ray	79.824	0.0798	0.162
				x-ray	80.255	0.0803	0.311
				x-ray	82.473	0.0825	0.112
		total:	**103.913**			total:	**100.224**

HS film: Expanded Stent	HS film: Unexpanded Stent	HD-810 film: Unexpanded Stent
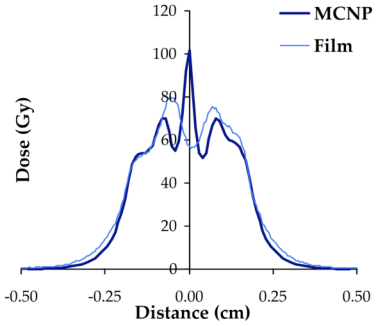 a: Transverse in contact.	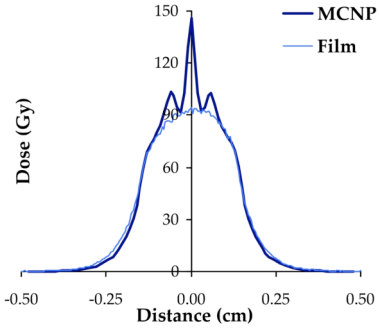 b: Transverse in contact.	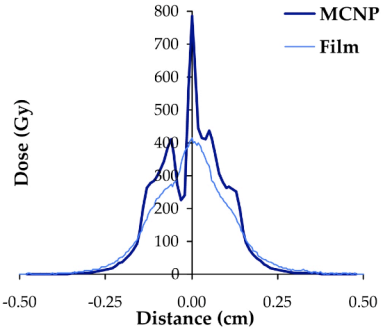 c: Transverse in contact.
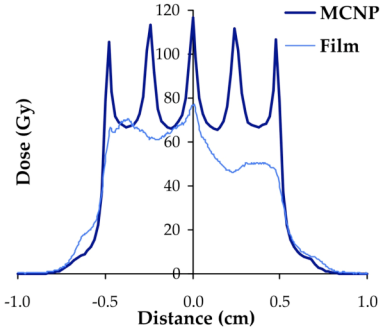 d: Along in contact.	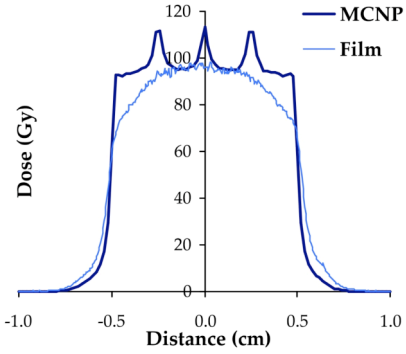 e: Along in contact.	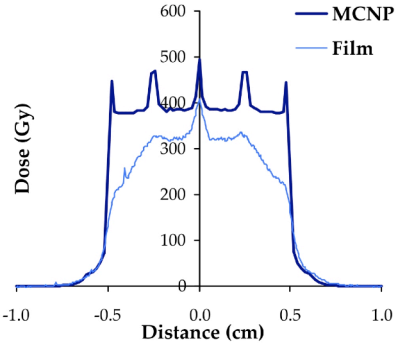 f: Along in contact.

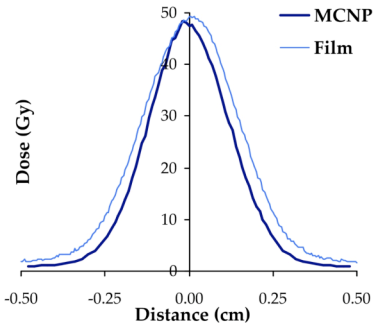

g: Transverse, 1 mm distant.

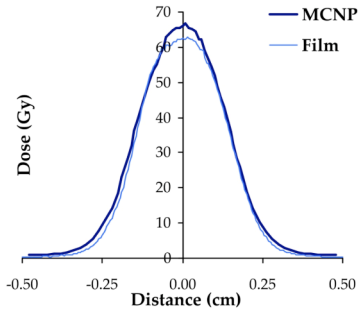

h: Transverse, 1 mm distant.

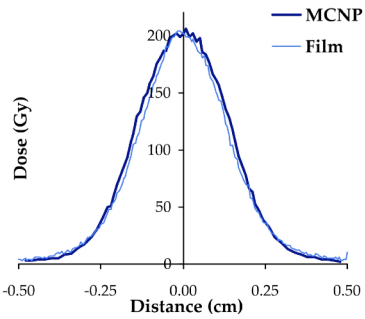

i: Transverse, 1 mm distant.

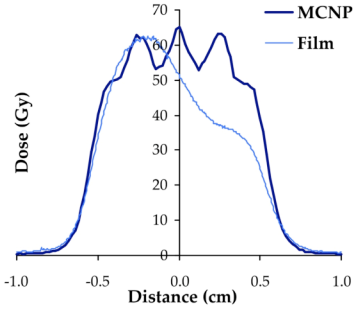

j: Along, 1 mm distant.

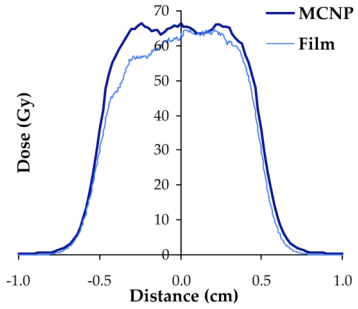

k: Along, 1 mm distant.

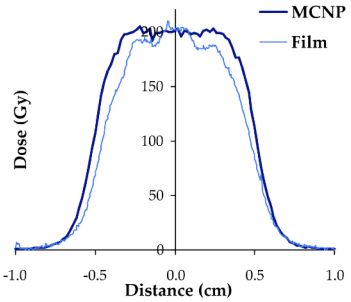

l: Along, 1 mm distant.

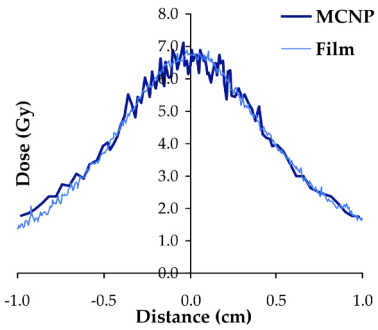

m: Transverse, 4 mm distant – Expanded.

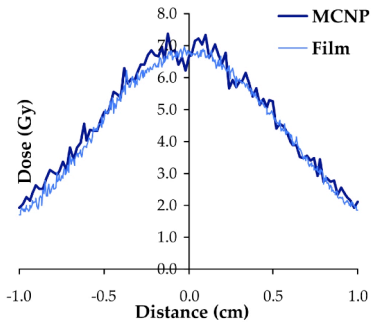

n: Along, 4 mm distant – Expanded.

Figure 15. Comparison of radiochromic film measurements and Monte Carlo simulations for expanded and unexpanded stents, for the film in contact with the stent, at 1 mm and 4 mm distant from the stent surface. Figures m and n are both for the expanded stent.

4. Validation of Struxel-based Dosimetry:

The stent used in the previous experiment was conceptually broken into pieces (struxels) as would be seen in transverse images in IVUS. Figure 16b shows these sectioning. The dose distribution at the films was calculated as the summation of the contributions from each of the struxels. Figure 16c and 16d show the comparison of the resultant dose calculations with the Monte Carlo simulation of the entire stent and the film measurements, as seen in Figure 15. In contact, the differences in the dose distribution resulting from the segmentation of the stent appear clearly, although by 1 mm away from the stent, the segmented calculation and the Monte Carlo simulations approximate each other. Some finer structure seen in the Monte Carlo is lost in the segmented calculation, however, that structure is not duplicated well in the actual measurements. The conclusion would be that except for calculation points closer than about 0.5 mm to the stent, the segmentation approach approximates the dose distribution adequately.

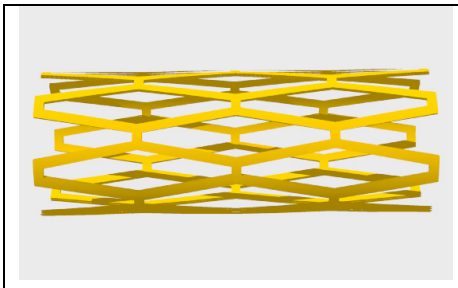

a

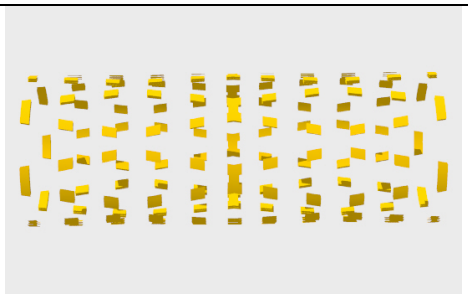

b

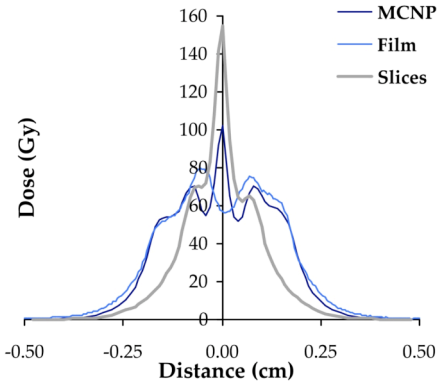

c. Transverse in contact.

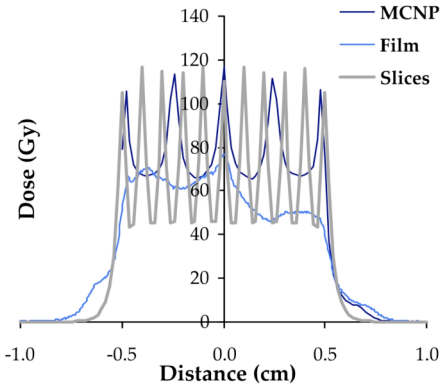

d. Along in contact.

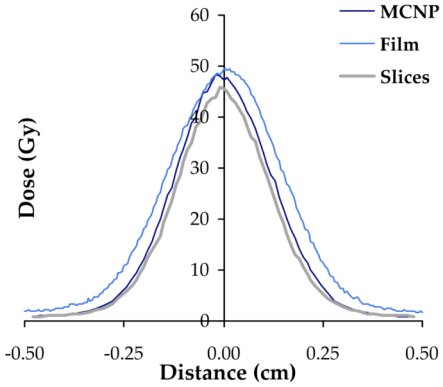

e: Transverse, 1 mm distant.

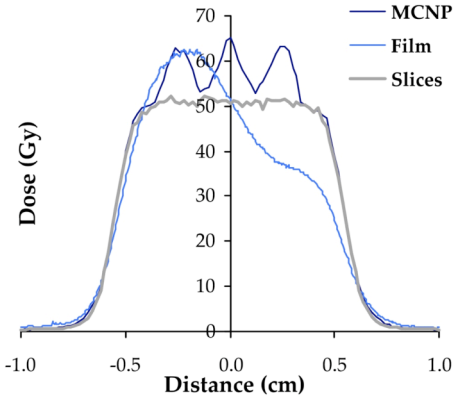

f: Along, 1 mm distant.

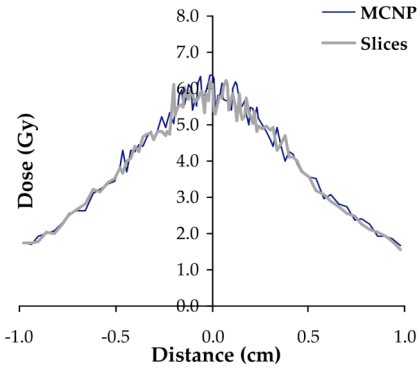

g: Transverse, 4 mm distant.

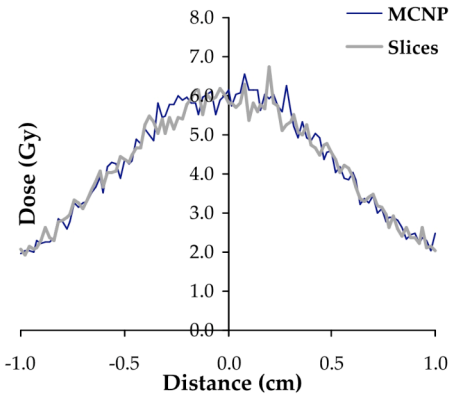

h: Along, 4 mm distant.

Figure 16 (previous page). Simulation of a radioactive stent by struxels in image planes: a. a schematic of the expanded stent, b. the expanded stent decomposed into the imaged struxels, c - h. comparison with film measurements and Monte Carlo in the transverse plane in contact with the stent.

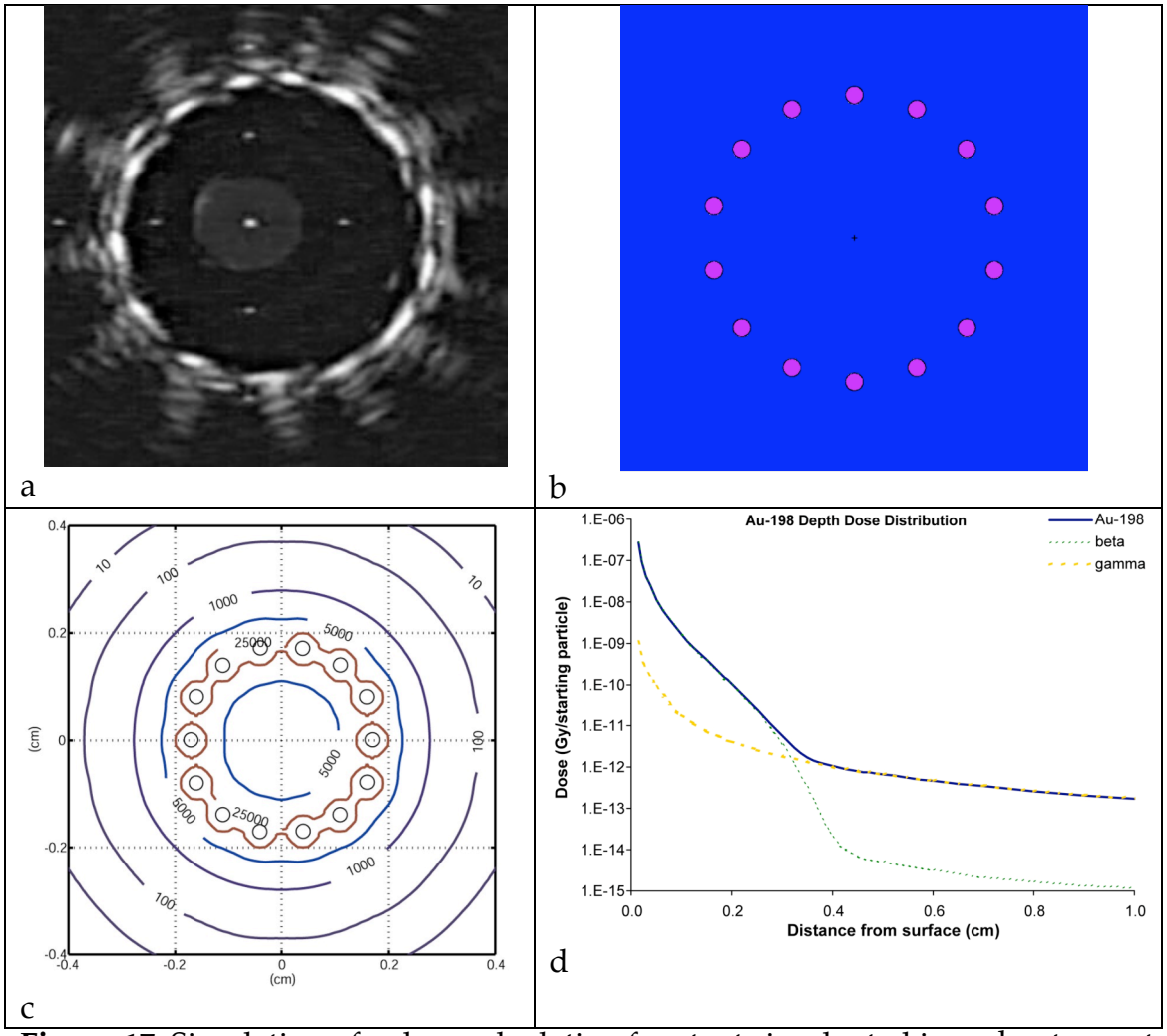

Figure 17. Simulation of a dose calculation for stents implanted in a phantom artery: a. The image of the implanted stents using IVUS, b. how the stent was represented in the calculational simulation, c. the dose distribution in one plane, d. the radial dose distribution.

5. Dose Image and Calculation 1 – Phantom Study:
Once the calculations were verified, two stents, a Crown stent and a Palmaz-Schatz P104 inserted into an "artery" in a phantom especially constructed to simulate coronary arteries for ultrasound imaging.[a] The phantom is an acrylic box filled with gelatin laced with graphite to give some scatter for the ultrasound. A 3mm inner diameter latex tube

[a] Phantom designed and constructed by Ernie Madsen, Gary Frank and Steve Peterson, University of Wisconsin.

running across the box mimics an artery. The intravascular ultrasound (IVUS) image is shown in Figure 17. Also shown in Figure 17 is the representation of the stent as identified in the imaging cuts as used in the dose calculation, and the calculated dose distribution. This experiment indicates that the image-based, segmentation approach would be feasible in a clinical setting.

6. Dose Image and Calculation 1 – Patient Study:
The last experiment was to attempt dosimetry on actual patient data. Images of an implanted stent after an angioplastic procedure were acquired using Intravascular Ultrasound (IVUS). IVUS images are taken with a small, rotating ultrasonic transducer that is inserted into the artery through a catheter. These images, recorded onto a VHS tape, were digitized and imported into the computer. The images were cleaned, aligned and entered into Pinnacle 6.2b (Philips, Milpitas, CA), treatment-planning software. These images gave representation of what the images of a radioactive stent would look like and allow simulation of a dose computation in a patient. From each slice, the pieces of the stent (struxel) were identified and marked as a cylindrical radioactive source with a diameter of 0.02 cm, a length of 0.01 cm and a 0.0001 cm layer of gold coating the outer radius of the cylinder. Using MCNP4c3, each "source" was modeled and the dosimetric information was calculated using TG-43 type characterization. These calculated dosimetric parameters were entered into the Pinnacle planning system. Figure 18 shows a dose calculation in a sample image section. The conclusion from this study is that *in-vivo* dosimetry for implanted radioactive stents based on IVUS images is indeed feasible.

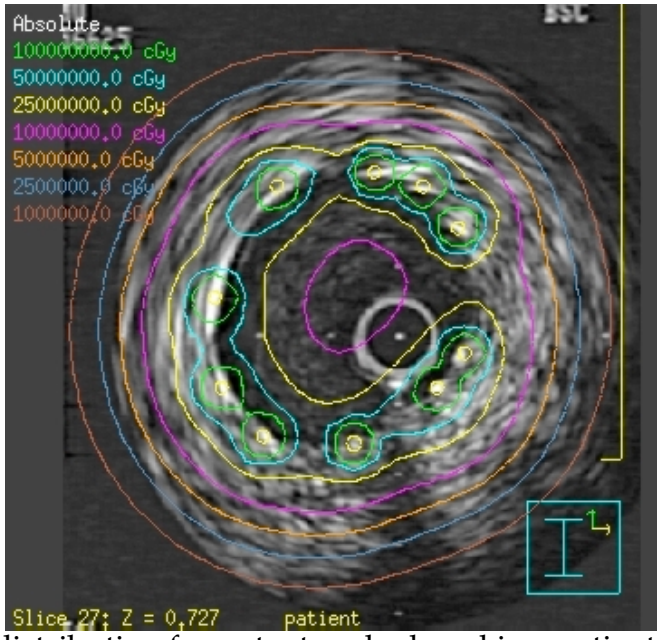

Figure 18. The dose distribution for a stent as deployed in a patient, ***were*** the stent radioactive. In the patient, this was a non-active stent.

Discussion

This project prepared the way for animal experiments to determine the optimum radionuclide for treatment to prevent restenosis. Such experiments are not likely to take place in the near future. Shortly after the beginning of this project, reports on drug-

coated stents were released. These stents were plated with chemotherapy agents in a timed-release form. The early results were outstanding, and they soon became available clinically, and interest in radioactive stents in the cardiology community disappeared. In practice, the drug-eluting stents fair slightly less well than in the pilot trials (which is always the case), and long-term results are not yet available. However, even if the results are worse than with radiation treatments, cardiologists are likely to still prefer the drug-coated stents because of the absence of radiation safety precautions. Should it turn out, however, that the long-term results fail to keep pace with the early results (also a very common phenomenon, and with some indications of such at the time of writing), the physical tools are ready for the commencement of animal experiments.

Even in the absence of renewed interest in radioactive stents, the work performed in this project will find application in brachytherapy. The radiolabeling techniques developed not only would be useful in the manufacture of other brachytherapy sources, but we have applied them in the development of brachytherapy sources with new characteristics (directionality of the emission pattern). The calibration techniques apply not only to the radioactive stents, but are now being applied for transcatheter intravascular brachytherapy (a therapeutic technique that remains in use, and with very poor calibration uncertainties before the methods developed in this project). Another project is underway to adapt the dose distribution calculational algorithm developed for the radioactive stents to ^{90}Y-labeled microsphere treatments for liver cancer. Thus, the spin-off from this project may have found application in areas with as much impact, and possibly more, than the original intention.

Reference

[1] AAPM Radiation Therapy Committee Task Group No. 60, R Nath, A Amols, C Coffey, D Duggan, S Jani, Z Li, M Schell, C Soares, J Whiting, P Cole, I Crocker, R Schwartz. Intravascular brachytherapy physics. Med. Phys. 26: 119 – 152 (1999)

[2] SJ Goetsch, FH Attix, SW Pearson, BR Thomadsen, Calibration of 192Ir high-dose-rate afterloading systems. Med Phys **18**, 462-467 (1991).

[3] S Kondo, M Randolph. 1960. Effect of finite size of ionization chambers of measurements of small photon sources. Radiation Research 13: 37 - 60 (1960)

[4] A Bielajew. Correction factors for thick-walled ionisation chambers in point-source photon beams. Phys Med Biol 35: 501 – 516 (1990).

[5] F Khan. *The Physics of Radiation Therapy*. (Baltimore: Williams and Wilkins, 1994).

[6] AAPM Radiation Therapy Committee Task Group 55, A Niroomand-Ran, CR Blackwell, BM Coursey, et al. Radiochromic Film Dosimetry. Med Phys 25: 2093 - 2115 (1998).